12th IFAC International Symposium on
Advanced Control of Chemical Processes
July 14-17, 2024. Toronto, Canada

Analysis of Aging in Lithium-ion Batteries: Fundamental Modeling and Parameter Investigation

Hyejung Oh [*], **Junseop Shin** [*], **Taekyu Kang** [**], **Woosung Kim** [**], and **Jong Min Lee** [*]

[*] *School of Chemical and Biological Engineering, Seoul National University, Seoul, Korea (e-mail: jongmin@snu.ac.kr).*
[**] *Battery Performance Technology Development Team, Hyundai Motor Company, Hwaseong-si, Gyeonggi-do, Korea*

Abstract: Lithium-ion batteries play a pivotal role in modern energy storage, offering high power, specific energy, and volumetric density, thereby establishing themselves as an eco-friendly alternative for diverse applications. As the demand for these batteries continues to grow, a comprehensive understanding of their intricate mechanisms becomes imperative. This study delves into the fundamental modeling of lithium-ion batteries, elucidating electrochemical processes and addressing aging complexities. Empirical models for Lithium-ion batteries, such as equivalent circuit models and open circuit voltage models, stand out for their real-time applications. Though these data-driven models achieve high accuracy and require low effort, their lack of explainability poses a limitation. Consequently, to comprehend the intricacies of batteries, it is essential to analyze the plausible causality inherent in internal electrochemical processes and aging effects, aspects challenging to capture in a simplified approach. This study, with a particular emphasis on aging, systematically scrutinizes model parameters, fitting them to experimental data, thereby unveiling subtle impacts on performance. The insights gained enhance predictive capabilities and contribute to the formulation of strategies for mitigating aging effects, ultimately extending the lifespan of lithium-ion batteries.

Keywords: Cell Modeling, Electric Vehicles, Lithium-ion Battery, Shepherd Model, Doyle-Fuller-Newman Model

1. INTRODUCTION

Lithium-ion batteries have emerged as a cornerstone in modern energy storage systems, serving diverse applications including portable devices, electric vehicles and renewable energy integration. Their high power, specific energy, and volumetric energy density, combined with compact sizing and low energy cost, position them as a revolutionary and environmentally friendly alternative to traditional internal combustion engines. As the demand for safe and efficient utilization of these batteries increases, a deeper understanding of their intricate mechanisms becomes imperative.

This study embarks on an exploration into the fundamental modeling of lithium-ion batteries, analyzing their dynamic electrochemical processes and addressing complex behaviors associated with aging phenomena. Fundamental modeling of lithium-ion batteries plays a pivotal role in comprehending the underlying behaviors that occur during their usage. By unraveling the intricate interplay of electrochemical reactions, transport phenomena, and material properties, researchers can get valuable insights persuing enhanced battery performance, longevity, and safety.

There have been active research efforts to understand the nature of lithium-ion batteries through modeling. They include equivalent circuit models(ECM) [Liaw et al. (2004)], empirical open-circuit voltage(OCV) models like the Shepherd model [Shepherd (1965); Tremblay and Dessaint (2009)] and the Nernst model [Verbrugge and Tate (2004)], and data-driven models that employ machine learning techniques [Wang et al. (2017)].

ECM regards the battery as an ideal power source connected to a circuit equivalent to the internal impedance and resistance, thereby managing computational demands [Lai et al. (2018)]. Empirical OCV models are the simplified version of modeling. As this method efficiently simulates voltage on a macroscopic scale, these OCV models are widely applied in industrial fields that require faster, near-real-time computation for control and optimization purposes [Raszmann et al. (2017)]. Li et al. (2019), Boujoudar et al. (2019), and Nascimento et al. (2021) studied data-driven approaches, using various deep-learning techniques and experimental data to simulate battery systems. Although these models show high accessibility and computational efficiency, they possess the disadvantage that they fail to provide enough description of the actual internal behavior of the battery during the charge and discharge process.

In terms of this interpretability, the models developed from fundamental principles exhibit much less limitations.

Governing Equation	Boundary Condition	
$\frac{\partial c_s}{\partial t} = \frac{D_s}{r^2}\frac{\partial}{\partial r}\left(r^2\frac{\partial c_s}{\partial r}\right)$	$\left.\frac{\partial c_s}{\partial r}\right\|_{x=0} = 0,\ -D_s\left.\frac{\partial c_s}{\partial r}\right\|_{r=R_s} = j_n$	(1)
$\epsilon_e\frac{\partial c_e}{\partial t} = \frac{\partial}{\partial x}\left(D_e\epsilon_e^p\frac{\partial c_e}{\partial x}\right) + \frac{3\epsilon_s(1-t_+^0)}{R_s}j_n$	$\left.\frac{\partial c_e}{\partial x}\right\|_{x=0} = \left.\frac{\partial c_e}{\partial x}\right\|_{x=L} = 0$	(2)
$\frac{\partial}{\partial x}\left(\sigma\epsilon_s\frac{\partial \phi_s}{\partial x}\right) = \frac{3\epsilon_s F}{R_s}j_n$	$\sigma\epsilon_s\left.\frac{\partial \phi_s}{\partial x}\right\|_{x=0} = \sigma\epsilon_s\left.\frac{\partial \phi_s}{\partial x}\right\|_{x=L} = \frac{i_{\text{app}}}{A_{\text{surf}}}$, $\left.\frac{\partial \phi_s}{\partial x}\right\|_{x=\delta_n} = \left.\frac{\partial \phi_s}{\partial x}\right\|_{x=L-\delta_p} = 0$	(3)
$\frac{\partial}{\partial x}\left(\kappa\epsilon_e^p\frac{\partial \phi_e}{\partial x} + \kappa\epsilon_e^p\nu\frac{2RT}{F}\frac{\partial lnc_e}{\partial x}\right) = -\frac{3\epsilon_s F}{R_s}j_n$	$\left.\frac{\partial \phi_e}{\partial x}\right\|_{x=0} = \phi_e\|_{x=L} = 0$	(4)
$j_n = \frac{i_0}{F}\left(exp\left(\frac{\alpha_a F}{RT}\eta\right) - exp\left(-\frac{\alpha_c F}{RT}\eta\right)\right)$ $i_0 = k_0 c_e^{\alpha_a}\left(c_s^{\max} - c_s^{\text{surf}}\right)^{\alpha_a}\left(c_s^{\text{surf}}\right)^{\alpha_c}$ $\eta = \phi_s - \phi_e - U$		(5)
$V(t) = \phi_s(L,t) - \phi_s(0,t) - \frac{R_{\text{film}}}{A_{\text{surf}}}i_{\text{app}}(t)$		(6)
$\frac{d\bar{c}_s}{dt} = \frac{-3}{R_s}j_n\ ,\ c_s^{\text{surf}} = \bar{c}_s - \frac{R_s}{5D_s}j_n$		(7)

Table 1. Governing equations used in Doyle-Fuller-Newman model

These models have diverse branches, such as Doyle-Fuller-Newman(DFN) model [Doyle et al. (1993)], Full Homogenized Model(FHM) [Arunachalam and Onori (2019)] and Single Particle Model(SPM) [Haran et al. (1998), Richardson et al. (2020)]. The full-scale DFN model is computationally intensive, and SPM and FHM reduce the spatial resolution to address this computational burden.

Lithium-ion batteries(LIBs), like other energy storage systems, undergo significant changes in performance characteristics over operation history due to aging factors. Therefore, this study mainly focuses on these changes, systematically analyzing model parameters closely related to the aging process of LIB based on the fundamental model.

The fundamental model was fitted to experimental data on a cycle-by-cycle basis, resulting in model parameter values corresponding to each cycle data. This allows us to investigate how the key parameters related to the battery's performance change over cycles. Then, each parameter was appropriately fitted as a function of cycles. By using parameters for the corresponding cycle numbers, the model can be applied to the actual usage of batteries. Insights obtained from this process could enhance the prediction of battery behavior and also contribute to the development of control strategies that alleviate the adverse effects of aging, thereby effectively managing the health and lifespan of LIBs.

The remainder of this paper is organized as follows: Section 2 will introduce the methods including the utilized dataset, model, and algorithm structure. The results are presented in Section 3. Finally, Section 4 wraps up the paper and suggests some future works.

2. METHODS

2.1 Dataset

The dataset utilized in this study was the battery dataset from the National Aeronautics and Space Administration's Prognostics Center of Excellence (NASA PCoE)[Saha and Goebel (2007)].

Each battery in this dataset independently underwent charge, discharge, and impedance measurement steps in various experimental settings, such as diverse discharge termination criteria and ambient temperature measurements. Only the discharge data were utilized, and each discharge cycle data consists of voltage, current, and temperature. The utilized discharge data were obtained from several constant current conditions, under the ambient temperature of 24 °C, and their battery indices were 5, 6, 7, 18, 33, 34, and 36(B0005, ..., B00036). A total of 168 discharge cycles exist for B0005 data, and the voltage, current, and temperature of each discharge cycle were plotted in Fig. 1.

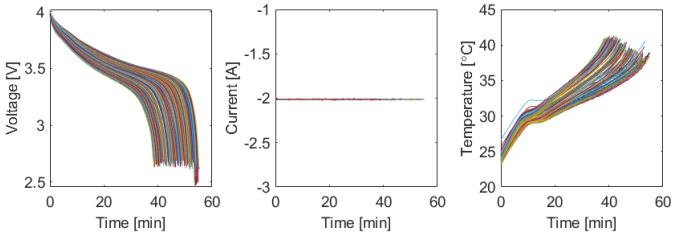

Fig. 1. Voltage, current, and temperature of each discharge cycle (168 cycles in total) in NASA PCoE B0005 data.

2.2 Doyle-Fuller-Newman(DFN) Model

Among various models introduced in Section 1, we adopted the DFN model in order to retain the physical explanation as much as possible in this study.

DFN model assumes that the electrode is a porous structure and that the geometry of the electrode's active materials are sphere. Fig. 2 presents a clear illustration of the system. The transport of lithium ion, and the resulting concentration and potential changes are fundamentally modeled based on first principles calculations.

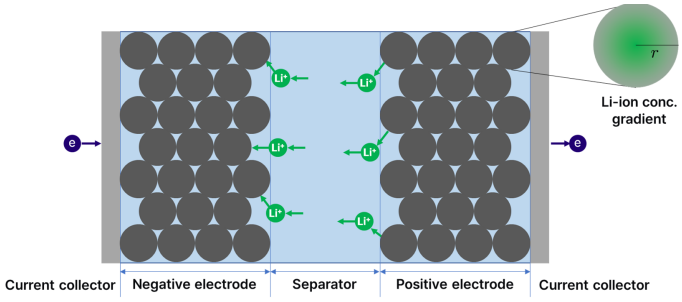

Fig. 2. Simple illustration of Doyle-Fuller-Newman model system. Active materials within the porous electrodes are assumed to have a uniform spherical shape within each electrode.

The governing equations consisting DFN model are listed in Table 1, and the notations are summarized in Table 2.

In Table 1, Eqs. 1 and 2 explain the changes of lithium concentration in the active material (solid phase) and electrolyte (liquid phase), respectively. Similarly, Eqs. 3 and 4 describe how the potential distribution changes within the active material and electrolyte. Eq. 5 is the Butler-Volmer kinetics, Eq. 6 calculates the cell voltage, and Eq. 7 is a relation for the simplification of the solid phase ion concentration. Assuming that the concentration inside the spherical active material follows a parabolic distribution, the radial dependence of the solid phase concentration can be eliminated by defining separate variables for the surface and bulk concentrations.

2.3 Temperature model

The temperature was calculated as a lumped parameter for the cell, solving the differential equation described in Eqs. (8) - (10).

$$\dot{Q}_{\text{conv}} = hA_{\text{heat}}(T_{\text{amb}} - T) \tag{8}$$

$$\dot{Q}_{\text{gen}} = i_{\text{app}}(U - V) - \text{Vol}_{e,b}Fa_s j_n T\frac{\partial U}{\partial T} \tag{9}$$

$$\frac{dT}{dt} = \frac{1}{mC_p}(\dot{Q}_{\text{conv}} + \dot{Q}_{\text{gen}}) \tag{10}$$

Notation	Variable Name
A_{heat}	Heat exchange area [m^2]
A_{surf}	Electrode area [m^2]
a_s	Specific surface area per unit volume ($= \frac{3\epsilon_s}{R_s}$) [1/m]
C_p	Heat capacity of the battery [J/K]
c	Lithium-ion concentration [mol/m^3]
$\bar{c}$	Bulk Li concentration [mol/m^3]
$c^{\max}$	Maximum Li concentration [mol/m^3]
c^{surf}	Li conc. at solid-electrolyte interface [mol/m^3]
D	Diffusion coefficient [m^2/s]
F	Faraday constant [C/mol]
h	Heat transfer coefficient[$W/(m^2 \cdot K)$]
i_0	Exchange current density [A/m^2]
i_{app}	Applied current [A]
j_n	Lithium flux [$mol/(m^2 \cdot s)$]
k_0	Kinetic constant
L	Total thickness ($= \delta_n + \delta_s + \delta_p$) [m]
m	Mass of the battery [kg]
p	Bruggeman exponent
$\dot{Q}_{\text{conv}}$	Convection heat transfer rate [J/s]
$\dot{Q}_{\text{gen}}$	Heat generation rate [J/s]
R	Gas constant [$J/(mol \cdot K)$]
R_{film}	Film resistance [$\Omega \cdot m^2$]
$R_{f,n}$	SEI resistance [$\Omega \cdot m^2$]
R_s	Radius of the active material particle [m]
T	Cell temperature [K]
T_{amb}	Ambient temperature [K]
t_+^0	Transference number
U	Open circuit voltage [V]
V	Cell voltage [V]
$\text{Vol}_{e,b}$	Electrode bulk volume [m^3]
α_a	Anodic charge transfer coefficient
α_c	Cathodic charge transfer coefficient
δ	Electrode thickness [m]
ϵ	Volume fraction
η	Overpotential [V]
κ	Ionic conductivity [S/m]
ν	Thermodynamic factor
σ	Electrical conductivity [S/m]
ϕ	Potential [V]
	Subscript
s	Active material (Solid phase) OR Separator
e	Electrolyte (Liquid phase)
n	Negative electrode
p	Positive electrode

Table 2. Notations for the Doyle-Fuller-Newman and temperature model

2.4 Algorithm

We developed a model from the DFN implementation by Khalik et al. (2021). The flow chart describing the scheme is described in Fig. 3. Since electrochemical and transport phenomena demonstrate the physical mechanism of the batteries, physical properties like diffusion coefficients, conductivities, and resistances were selected as key parameters to be analyzed. The list of all physical properties optimized is presented in Section 3.1. The parameter identification was achieved by minimizing the 2-norm loss between the experimental data and DFN model's voltage and temperature. The optimization was performed via MATLAB, `lsqnonlin` function on a cycle-by-cycle basis. The constraint was set on each physical property, based on previous studies or around the literature values. More specifically, the loss function described in Fig. 3 considers both voltage and temperature for accurate prediction on both features. To achieve effective fitting, min-max scaling was applied separately on voltage and temperature, to ensure their contribution to the loss function remains comparable.

The design for the loss function was critical for both enhancing the accuracy of the final optimization result and ensuring that the optimization itself proceeds. Parameter guesses that deviate significantly from the accurate value may lead to the simulation to terminate prematurely due to violations of physical boundaries. Forcing a 2-norm calculation despite length differences results in `NaN` values. To properly formulate the loss function, one option can be to assign a constant high value for such prematurely terminated cases. This will be appropriate for the initial values near the true parameters.

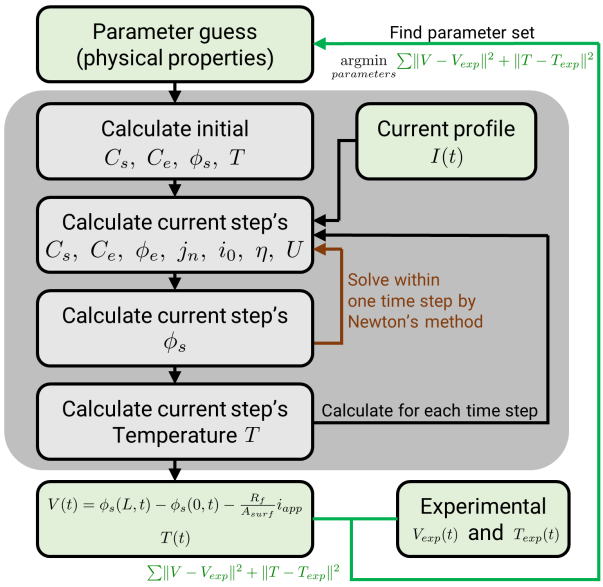

Fig. 3. The flowchart for finding parameters for the Doyle-Fuller-Newman model. Simulations were conducted by the DFN model(shaded region) with each parameter guesses, and 2-norm losses were minimized with respect to parameters.

However, when the initial values are significantly distant from the true values, there will be no loss gradient, as every parameter guess results in premature termination. When various experimental data are used for parameter evaluation, it is difficult to provide accurate initial values for every experiment, which involves understanding a system with multiple coupled differential equations. Therefore, zero padding for the prediction values after the termination was applied to generate loss gradients toward the true property value.

The first three and last three cycles were picked as representatives, and a simultaneous optimization was conducted for the representative cycles of all batteries at 24°C. The resulting parameters of this simultaneous optimization were utilized as initial values for optimizations of individual cycles. After this process, the effect of cycle number on physical properties was investigated.

3. RESULTS AND DISCUSSION

3.1 Finding physical properties for independent cycles

Optimizations were conducted for each cycle of B0005 data to obtain physical property parameters. The optimized physical property parameters can be categorized into the following five sections.

1) Stoichiometry of positive and negative electrodes at 0% and 100% SoC ($s_{0,p}$, $s_{0,n}$, $s_{100,p}$, $s_{100,n}$),

2) Diffusion coefficients of positive and negative electrodes and the electrolyte ($D_{s,p}$, $D_{s,n}$, D_e),

3) Positive and negative electrode conductivity as well as ionic conductivity (σ_p, σ_n, κ)

4) Resistances related to SEI film formation in the negative electrode and the current collector interface. Denoted as one symbol R_{film} in Table 1. ($R_{f,n}$, R_{cc})

5) Heat transfer coefficient and heat capacity, which are related to temperature dynamics (h, C_p).

These properties were then re-applied to the DFN model for validation. The Root Mean Square Error (RMSE) was calculated for each cycle, yielding an average RMSE of 0.0780 V and 0.4978 K for voltage and temperature, respectively.

The experimental data and model output of the first cycle are displayed in Fig. 4, while those of the 121st cycle are shown in Fig. 5.

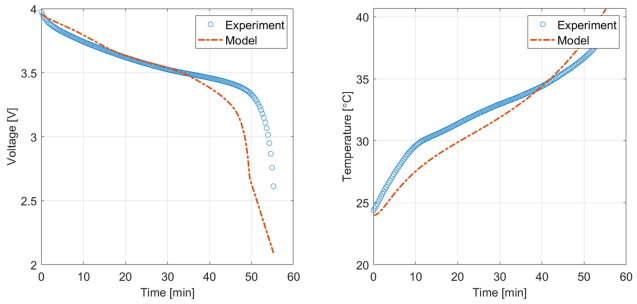

Fig. 4. The experimental data and model output for the first discharge cycle of B0005. The calculated RMSE values for voltage and temperature were 0.2603 and 1.3485, respectively. A relatively high loss value compared to the later cycles is believed to stem from the initial relaxation of the cell.

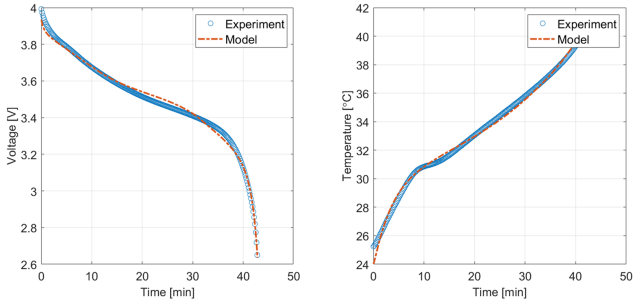

Fig. 5. The experimental data and model output for the 121st discharge cycle of B0005. The calculated RMSE values for voltage and temperature were 0.0221 and 0.2501, respectively.

More specifically, for the early cycles, the experimental data points and the simulation results were not very close, but the accuracy improved towards the later cycles.

There are two possible reasons for this. First, the optimal property parameters for the early stages may lie outside the minimum and maximum values assigned for each physical property. In other words, the optimization may have been blocked at the boundary. However, the probability of this reason is somewhat low, since there were few improvements even when the boundary limits were loosened into barely physical regions. The second reason can be the various initial cell relaxation phenomena

with several time constants [Fuller et al. (1994); Peled and Menkin (2017)]. The radical discharge behaviors can be observed in the early cycles, therefore this radical behavior can be the reason for the relatively large gap between the experimental data and model output.

3.2 Analysis on parameter changes over cycles

Important changes in parameters were plotted and regressed in Figure 6. Since the obtained properties did not predict the voltage and temperature for early cycles accurately, the properties after the 50th cycle were regarded as meaningful and were plotted.

The overall trend observed for diffusion coefficients was a decrease in exposure time for the charge and discharge loads, as well as the conductivities. Resistance values, namely $R_{f,n}$ and R_{cc}, increased with each cycle. The decrease in the diffusion coefficient for the negative electrode suggests that the solid electrolyte interface(SEI) impedes the diffusion of lithium ions. Although the increase in the diffusion coefficient of the positive electrode in the later cycle could be attributed to surface stabilization and increased overall temperature, additional analysis is required to explore other possible causes. Similar behavior that appeared in the electrolyte phase seems to be caused by electrolyte decomposition resulting from repeated cycles of charging and discharging[Kabir and Demirocak (2017)]. The overall decrease in conductivity can be traced to changes in local electronic structure [Nagpure et al. (2011), Kleiner et al. (2015)] and side reactions such as transition metal loss from the positive electrode and development of passivation layers. For resistances, there is an obvious increase in $R_{f,n}$ since it represents the SEI film resistance at the negative electrode. Furthermore, the corrosion and oxidation of the current collector can explain the increase in R_{cc}. The observed increase in both resistance values, which are the internal resistances of the battery, with cycle number matches the tendency of heat generation to increase with each cycle.

B0006 was chosen to evaluate the obtained parameter fittings for the reliability of the unseen batteries. The experimental conditions for B0005 and B0006 were identical except for the criteria for the discharge termination. The criterion was at 2.7V battery voltage for B0005 and 2.5V for B0006.

The model using parameters from B0005 data was simulated following the operation condition of the B0006 experiment. The results were compared with the experimental data of B0006 and shown in Fig. 7. The RMSE was calculated for each cycle, and the average was 0.2497 V for voltage and 1.1925 K for temperature. A fundamental model like DFN is highly interpretable since it has internal calculations that one can analyze step by step, but its physical property values either need to be gathered from the literature or obtained through measurement. If this separate experimental measurement for precise physical properties is challenging, it could be feasible to obtain physical properties through charge and discharge experiments on representative cells. Subsequently, the model can be applied using these properties when the battery operates under comparable circumstances.

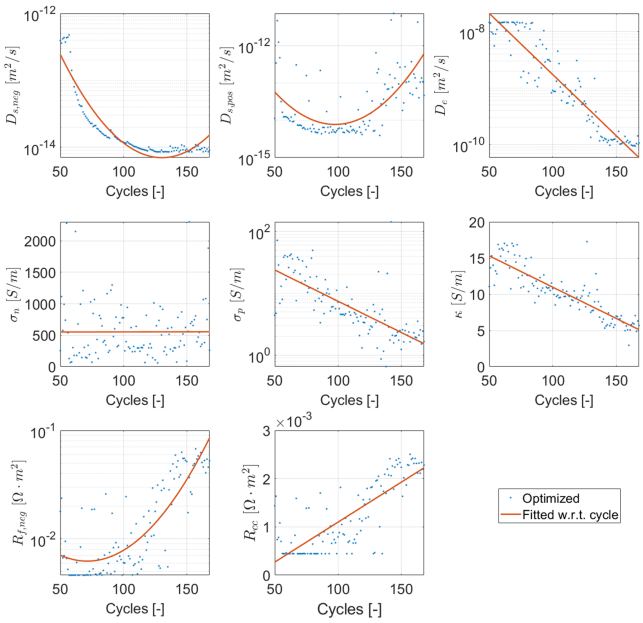

Fig. 6. The physical properties, input for DFN model, calculated from the optimization. These physical properties went through the regression with respect to cycle number.

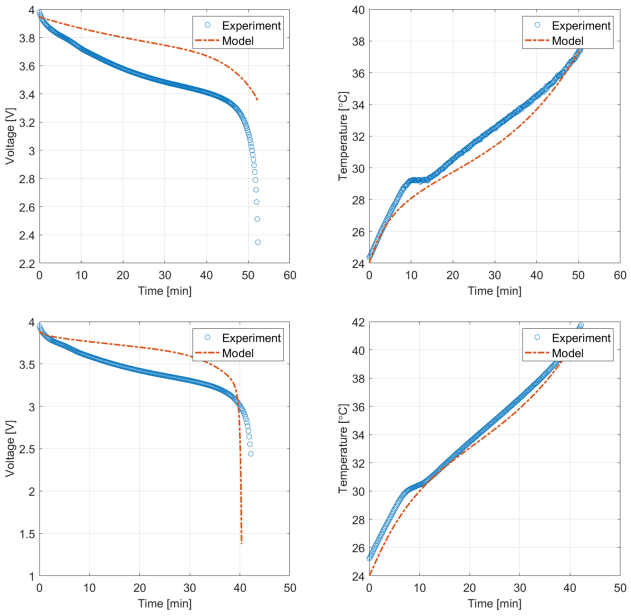

Fig. 7. The experimental data and model output for the 51st and 121st cycle of B0006. The regressed parameters obtained from B0005 were used.

4. CONCLUSION

We tried to get a peek into the internal dynamics of a LIB through the fundamental model. Without predefining the function form for the physical property change with respect to the cycle number, the physical properties for the DFN model were obtained through independent cycle-by-cycle optimization. Based on the observed trends, the discharge profile of another battery, which can be interpreted as unseen data, was simulated.

Further development of this parameter estimation process could provide valuable insight into the phenomena occurring within the battery, such as the SEI layer growing too much, without requiring physical disassembly of the battery. This can serve as additional information for battery replacement and also contribute to the design of more reliable and efficient control strategies.

Various future works are under consideration. First, conducting a thorough investigation of the initial relaxation process and adding this aspect into the model would enhance the performance for the early cycle. Next, in this study, B0005 and B0006 were treated as independent datasets that were comparable and used one of them for parameter fitting and the other one as unseen data. The conditions are indeed nearly identical in all aspects, including ambient temperature, number of cycles completed, and the load current value during constant current discharge. However, there is a slight difference between the datasets in terms of discharge-stopping criteria for each cycle. Therefore, it will improve the performance to apply the rainflow counting [Fioriti et al. (2023)] technique that considers the depth of discharge instead of just cycle count. Lastly, a performance rise can occur from conducting a parameter study that holistically considers the impact of other variables.

ACKNOWLEDGEMENTS

This research was financially supported by Hyundai Motor Company.

REFERENCES

Arunachalam, H. and Onori, S. (2019). Full homogenized macroscale model and pseudo-2-dimensional model for lithium-ion battery dynamics: comparative analysis, experimental verification and sensitivity analysis. *Journal of The Electrochemical Society*, 166(8), A1380.

Boujoudar, Y., Elmoussaoui, H., and Lamhamdi, T. (2019). Lithium-ion batteries modeling and state of charge estimation using artificial neural network. *International Journal of Electrical and Computer Engineering*, 9(5), 3415.

Doyle, M., Fuller, T.F., and Newman, J. (1993). Modeling of galvanostatic charge and discharge of the lithium/polymer/insertion cell. *Journal of the Electrochemical society*, 140(6), 1526.

Fioriti, D., Scarpelli, C., Pellegrino, L., Lutzemberger, G., Micolano, E., and Salamone, S. (2023). Battery lifetime of electric vehicles by novel rainflow-counting algorithm with temperature and c-rate dynamics: Effects of fast charging, user habits, vehicle-to-grid and climate zones. *Journal of Energy Storage*, 59, 106458.

Fuller, T.F., Doyle, M., and Newman, J. (1994). Relaxation phenomena in lithium-ion-insertion cells. *Journal of the Electrochemical Society*, 141(4), 982.

Haran, B.S., Popov, B.N., and White, R.E. (1998). Determination of the hydrogen diffusion coefficient in metal hydrides by impedance spectroscopy. *Journal of Power Sources*, 75(1), 56–63.

Kabir, M. and Demirocak, D.E. (2017). Degradation mechanisms in li-ion batteries: a state-of-the-art review. *International Journal of Energy Research*, 41(14), 1963–1986.

Khalik, Z., Donkers, M., and Bergveld, H.J. (2021). Model simplifications and their impact on computational complexity for an electrochemistry-based battery modeling toolbox. *Journal of Power Sources*, 488, 229427.

Kleiner, K., Melke, J., Merz, M., Jakes, P., Nagel, P., Schuppler, S., Liebau, V., and Ehrenberg, H. (2015). Unraveling the degradation process of lini0. 8co0. 15al0. 05o2 electrodes in commercial lithium ion batteries by electronic structure investigations. *ACS applied materials & interfaces*, 7(35), 19589–19600.

Lai, X., Zheng, Y., and Sun, T. (2018). A comparative study of different equivalent circuit models for estimating state-of-charge of lithium-ion batteries. *Electrochimica Acta*, 259, 566–577.

Li, S., He, H., and Li, J. (2019). Big data driven lithium-ion battery modeling method based on sdae-elm algorithm and data pre-processing technology. *Applied energy*, 242, 1259–1273.

Liaw, B.Y., Nagasubramanian, G., Jungst, R.G., and Doughty, D.H. (2004). Modeling of lithium ion cells—a simple equivalent-circuit model approach. *Solid state ionics*, 175(1-4), 835–839.

Nagpure, S.C., Babu, S., Bhushan, B., Kumar, A., Mishra, R., Windl, W., Kovarik, L., and Mills, M. (2011). Local electronic structure of lifepo4 nanoparticles in aged li-ion batteries. *Acta materialia*, 59(18), 6917–6926.

Nascimento, R.G., Corbetta, M., Kulkarni, C.S., and Viana, F.A. (2021). Hybrid physics-informed neural networks for lithium-ion battery modeling and prognosis. *Journal of Power Sources*, 513, 230526.

Peled, E. and Menkin, S. (2017). Sei: past, present and future. *Journal of The Electrochemical Society*, 164(7), A1703.

Raszmann, E., Baker, K., Shi, Y., and Christensen, D. (2017). Modeling stationary lithium-ion batteries for optimization and predictive control. In *2017 IEEE Power and Energy Conference at Illinois (PECI)*, 1–7. IEEE.

Richardson, G., Korotkin, I., Ranom, R., Castle, M., and Foster, J. (2020). Generalised single particle models for high-rate operation of graded lithium-ion electrodes: Systematic derivation and validation. *Electrochimica Acta*, 339, 135862.

Saha, B. and Goebel, K. (2007). Battery data set. NASA Prognostics Data Repository, NASA Ames Research Center, Moffett Field, CA.

Shepherd, C.M. (1965). Design of primary and secondary cells: Ii. an equation describing battery discharge. *Journal of the electrochemical society*, 112(7), 657.

Tremblay, O. and Dessaint, L.A. (2009). Experimental validation of a battery dynamic model for ev applications. *World electric vehicle journal*, 3(2), 289–298.

Verbrugge, M. and Tate, E. (2004). Adaptive state of charge algorithm for nickel metal hydride batteries including hysteresis phenomena. *Journal of Power Sources*, 126(1-2), 236–249.

Wang, Q.K., He, Y.J., Shen, J.N., Ma, Z.F., and Zhong, G.B. (2017). A unified modeling framework for lithium-ion batteries: An artificial neural network based thermal coupled equivalent circuit model approach. *Energy*, 138, 118–132.